

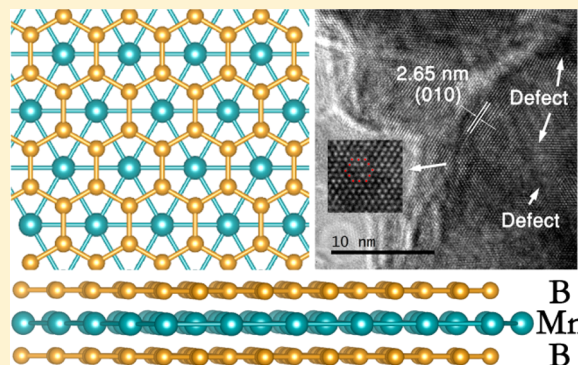
# Investigating Robust Honeycomb Borophenes Sandwiching Manganese Layers in Manganese Diboride

Shuailing Ma, Kuo Bao, Qiang Tao, Chunhong Xu, Xiaokang Feng, Pinwen Zhu, and Tian Cui\*

State Key Laboratory of Superhard Materials, Jilin University, Changchun 130012, China

## Supporting Information

**ABSTRACT:** We report a robust honeycomb boron layers sandwiching manganese layers compound,  $\text{MnB}_2$ , synthesized by high pressure and high temperature. First-principle calculation combined with X-ray photoelectron spectrum unravel that the honeycomb boron structure was stabilized by filling the empty  $\pi$ -band via grabbing electrons from manganese layers. Honeycomb boron layers sandwiching manganese layers is an extraordinary prototype of this type of sandwiched structure exhibiting electronic conductivity and ferromagnetism. Hydrostatic compression of the crystal structure, thermal expansion, and the hardness testing reveal that the crystal structure is of strong anisotropy. The strong anisotropy and first-principle calculation suggests that B–B bonds in the honeycomb boron structure are a strong directional covalent feature, while the Mn–B bonds are soft ionic nature. Sandwiching honeycomb boron layers with manganese layers that combine p-block elements with magnetic transition metal elements could endow its novel physical and chemical properties.



## INTRODUCTION

Because of C  $sp^2$  hybridization, two-dimensional (2D) honeycomb graphene exhibits high mechanical strength, outstanding electrical conductivity, and fantastic optical properties.<sup>1–5</sup> Electron-deficient boron element, like carbon, usually presents extraordinary chemical bonding flexibility features and formation of various structural complexities.<sup>6–11</sup> However, because of the empty  $\pi$ -valence band, 2D borophenes with honeycomb structure are inherently instable.<sup>10,12</sup> To fill the  $\pi$ -valence band of honeycomb of boron, every boron atom needs one more electron to reach  $s^2p^2$ . Consequently, honeycomb borophenes are still out of our sight. Recently, Mannix et al. synthesized 2D borophenes on silver surface under ultrahigh vacuum conditions.<sup>11,13</sup> However, the synthesized borophenes do not crystallize in a honeycomb crystal structure.

Nevertheless, the graphene-like honeycomb structure boron layers usually emerged in the metal diborides. On the basis of Korringa–Kohn–Rostoker (KKR) calculations and the X-ray photoelectron spectrum (XPS) measurements, Ihara, Hirabayashi, and Nakagawa proposed that the bonding nature of metal diborides can be explained by a combination of the honeycomb boron network bonding model and hcp-transition metal (TM) layers.<sup>14</sup> Thus, metal diborides usually possess both the properties of borophenes and the properties of metal layers.<sup>15</sup> Therefore, 2D borophenes interlayered with metal layers may exhibit exotic properties, including ultrahigh-temperature ceramics (UHTCs; e.g.,  $\text{WB}_2$ ),<sup>16</sup> high-temperature superconducting (e.g.,  $\text{MgB}_2$ ),<sup>17</sup> Dirac cones (e.g.,  $\text{MoB}_4$ ),<sup>18</sup> and magnetic (e.g.,  $\text{CrB}_2$ ).<sup>19</sup> The reason for the emergence of honeycomb borophenes in the metal diborides is still a mystery

and is useful to instruct synthesizing honeycomb borophenes. Furthermore, aborative selection of metal layers could stabilize the graphene-like honeycomb boron layers and bring superconducting and ferromagnetism. Manganese atoms possess many oxidation states (+2, +3, +4, +6, +7). The high capacity of manganese element to provide electron may ensure the filling of  $\pi$ -bands of 2D honeycomb boron layers. As it is known, manganese atom is a peculiar spin-polarized ion and has many-body physical properties and fantastic chemical behaviors. Manganese compounds generally exhibit exotic magnetic properties, such as super-paramagnetic (e.g.,  $\text{Mn}_3\text{O}_4$ ),<sup>20</sup> colossal magnetoresistance (e.g.,  $\text{La}_{0.67}\text{Ca}_{0.33}\text{MnO}_3$ ),<sup>21</sup> ferromagnetic (e.g.,  $\text{MnB}$ ),<sup>22</sup> and spin glass (e.g.,  $\text{CuMn}$ ).<sup>23</sup> Manganese diborides exhibit the above structure of 2D borophenes interlayered with honeycomb manganese laminar layers in sequence ...AHAHAH..., which is the prerequisite to investigate this exotic structure.<sup>24–27</sup> Thus, honeycomb boron layers sandwiching manganese layers may impart some fantastic physical properties. In a word, investigation of the electronic structure and bond structure is meaningful to understand the emergence of honeycomb borophenes in this crystal structure and to explore the properties of it.

In this work, robust covalent graphene-like honeycomb boron layers and metallic manganese layers are glued together by ionic bonds to form manganese diborides synthesized by high pressure and high temperature. The emergence of

Received: July 22, 2016

honeycomb boron layers was explored by combining XPS and first-principle calculation. The strength of laminar boron sheets tends to be robust, which is determined by thermal expansion, high pressure compress, and hardness measurements. Moreover, it is highly desirable to expect novel or enhanced electronic, magnetic, spintronic, catalytic, and mechanical properties.

## EXPERIMENTAL AND COMPUTATIONAL DETAILS

The raw materials were prepared by grinding the powders of pure manganese (99.95% in purity) and amorphous boron (99.5% in purity) with a ratio of 1:3 with an agate mortar and pestle until a uniform mixture was achieved. The raw materials of the mixed powders were cold-pressed into a 4 mm in diameter and 2.5 mm in height cylindrical pellet by hydraulic press. The hexagonal BN capsule was used as an insulation material to prevent the raw materials from reacting with the carbon heater that was placed in the MgO tube. The pure sample was synthesized on an SPD 6 × 600 T cubic anvil apparatus at a temperature 1600 to 2200 K and a pressure of 5.0 GPa with a duration time of 20 min. Finally, the sample temperature was quenched to room temperature by switching off the power supply.

As the bulk sample was synthesized, the sample was ground into powder with agate mortar. The phase of the as-synthesized sample was characterized by X-ray diffraction using Cu K $\alpha$  ( $\lambda = 0.1504 \text{ \AA}$ ) radiation by Rigaku D/max-2005 X-ray diffractometer. The crystal structure parameter of MnB<sub>2</sub> was determined by analyzing the collected X-ray diffraction data with GSAS program suite. The morphology and chemical composition of the as-synthesized samples were studied by means of the scanning electron microscopy (SEM; Maglan400) equipped with energy-dispersive spectrometer (EDS). The sample for transmission electron microscopy (TEM) was prepared by striking the material with a hydraulic press, and the obtained material was ultrasounded with alcohol. Then, the suspension solution was deposited on a holey carbon grid. The selected area electron diffraction (SAED) patterns and high-resolution TEM (HRTEM) images were acquired by JEM-2200FS. The microhardness of the sample was investigated by HV-1000ZDT microhardness tester, and the applied load  $P$  and  $H_v$  were determined using

$$H_v = 1.8544 \times P/d^2$$

where  $d$  is the mean of the two diagonals of the indentation, and  $P$  is the applied load with a holding time of 15 s. The SEM equipped with EDS was used to analyze whether the indentation is on the manganese diborides. XPS measurements were performed with an X-ray source equipped with a Mg anode ( $h\nu = 1253.6 \text{ eV}$ ) in an ultrahigh vacuum (UHV) chamber at a base pressure of  $1 \times 10^{-10}$  mbar. The fracture surface of the cylindrical specimen was cleaned by the Ar<sup>+</sup> sputtering with 180 s.

The Vienna ab initio simulation program (VASP) code with pseudopotentials plane-wave method was employed to conduct first-principle calculations of MnB<sub>2</sub>.<sup>28</sup> The exchange-correlation functional was taken into account through Perdew–Burk–Ernzerhof (PBE) exchange-correlation function in the generalized gradient approximation (GGA).<sup>29</sup> A plane-wave cutoff of 500 eV and a dense Monkhorst–Pack grid with a reciprocal space resolution of  $2\pi \times 0.03 \text{ \AA}^{-1}$  were chosen to ensure the total energies are convergent within 1 meV/atom. Elastic constants were calculated using strain–stress method, based on which the mechanical properties of bulk modulus and shear modulus were obtained via the Voigt–Reuss–Hill (VRH) approximation. Mulliken populations were calculated by the density-functional plane-wave technique using a  $2 \times 2 \times 2$  supercell implemented in the CASTEP code.<sup>30,31</sup> The ultrasoft Vanderbilt pseudopotentials (USPP) with GGA-PBE are chosen, and the cutoff energy is 300 eV with the k-mesh  $2\pi \times 0.03 \text{ \AA}^{-1}$ .

## RESULTS AND DISCUSSION

To prepare monophasic AlB<sub>2</sub>-type MnB<sub>2</sub>, excess amorphous boron powder, which cannot be detected by X-ray diffraction,

and manganese powder with a ratio of 1:3 were mixed to the raw materials. Figure S1 shows the X-ray diffraction patterns of the synthesized samples at different temperature. The Mn<sub>3</sub>B<sub>4</sub> and MnB<sub>4</sub> were synthesized below the temperature of 1800 K, and pure manganese diboride was synthesized above the temperature of 1850 K. As the temperature is above 2200 K, some tiny diffraction peaks appear, which may stem from the crystallization of amorphous boron at high temperature. The powder diffraction pattern of MnB<sub>2</sub> synthesized at the temperature of 1900 K demonstrates that this specimen synthesized by high pressure and high temperature is highly crystalline as shown in Figure 1, and no lines of impurities were

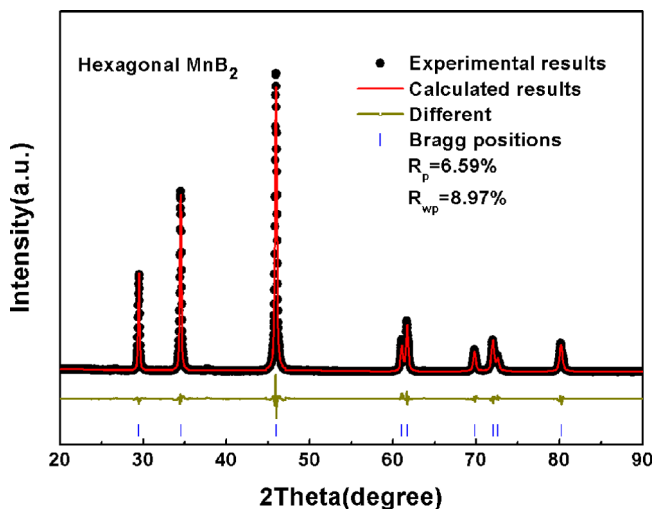


**Figure 1.** Rietveld refinement pattern of the MnB<sub>2</sub>. Solid dots: observed results; red line: calculated curve; blue vertical line: Bragg positions; dark yellow line: the different curve between the observed and the calculated curve.

detected. The diffraction pattern matches fairly well with the existing reference data available for this crystal from the Joint Committee on Powder Diffraction Standards (JCPDS No. 65–7346).

The crystal structure of MnB<sub>2</sub> was determined by the Rietveld refinement, and the crystal structure was depicted in Figure 2a,c. The crystal structure reveals that there are honeycomb boron layers sandwiching manganese layers. According to the previous results, TM diborides normally

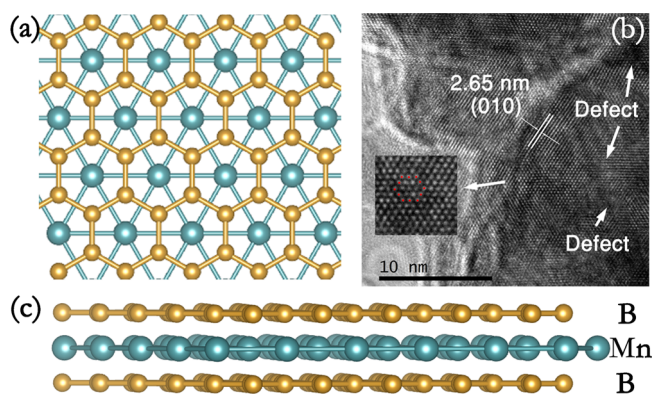


**Figure 2.** (a, c) The crystal structures of the AlB<sub>2</sub>-type MnB<sub>2</sub>. The blue spheres represent Mn atoms, and the dark yellow spheres represent the B atoms. (b) High-magnification HRTEM images of MnB<sub>2</sub>.

crystallize in a representative layered hexagonal  $AlB_2$ -type structure if the ratio of  $R_{TM}/R_B$  is in the range from 1.14 to 2.06, where  $R_{TM}$  and  $R_B$  refer to the atomic radii of TM and boron atoms, respectively.<sup>32</sup> The  $R_{TM}/R_B$  ratio of manganese and boron atoms is 1.85, which satisfies the above criterion. Consequently,  $MnB_2$  adopts hexagonal sandwiching-type structure. The obtained crystal information on  $MnB_2$  is compiled in the Table 1. The sandwiching crystal structure

**Table 1. Experiment Data and the Crystal Details Obtained from the Rietveld Refinement**

identification code	$MnB_2$		
formula weight	76.56		
radiation	Cu $K_\alpha$		
wavelength (Å)	1.5418		
crystal system	hexagonal		
space group	$P6/mmm$		
unit cell dimensions (Å)	$a = b = 3.0174(3)$ $c = 3.0397(5)$		
	$\alpha = \beta = 90^\circ$		
	$\gamma = 120^\circ$		
volume (Å <sup>3</sup> )	23.862		
density (calculated) (g/cm <sup>3</sup> )	5.095		
$\Theta$ range/deg	20–90		
	$R_p = 0.0659$		
residuals	$R_{wp} = 0.0897$		
	$\chi^2 = 2.851$		
atomic position	Wyckoff	(x, y, z)	occupancy
Mn	1a	(0, 0, 0)	0.9221
B	2d	(1/3, 2/3, 1/2)	1

depicted in Figure 2a,c possesses the following lattice parameters:  $a = b = 3.0113$  Å and  $c = 3.040$  Å, which matches fairly well with the previously reported results. On the basis of the Pearson's structure stable criterion, for the stable layered  $AlB_2$  type of  $TMB_2$ , the ratio of crystal lattice parameters  $c/a$  must be in the range from 0.59 to 1.2.<sup>32</sup> Thus, from the Rietveld refinements results, the ratio of  $MnB_2$  is 1.007, also hinting that this structure is definitely stable. However, according to the Rietveld refinement, the perfect  $MnB_2$  crystal diffraction matches the observed diffraction pattern with large errors, but the partial occupying of manganese atoms in the  $MnB_2$  to form  $Mn_{1-x}B_2$  is more favorable. This result is compatible with later EDS and HRTEM results. Note that, in the  $AlB_2$ -type manganese diboride, manganese layers are accommodated as alternating layers along  $c$ -axis and the graphene-like boron planes located between manganese planes in sequence... AHAAH... As seen in Figure 2a,c, the boron atoms are located at the corners of hexagon with nine neighboring atoms, six manganese atoms, and three boron atoms. The manganese atoms are arranged at the middle of adjacent boron layers right in the center of boron hexagons. Consequently, the manganese atoms and boron atoms have  $[MnB_{12}Mn_8]$  and  $[BMn_6B_3]$  coordination patterns, respectively. The atomic distance of the B–B bond is 1.703 Å in the honeycomb boron layer, which is smaller than that in the rhenium diboride.<sup>26</sup> The most interesting feature of this structure is that honeycomb boron layers sandwich the manganese layers with weak ionic interaction. This exotic structure opens a gate to investigate honeycomb boron layers and manganese layers.

To investigate the morphology of the synthesized specimen, the fracture surface of the cylindrical specimen was observed by SEM. As can be seen in the SEM low-magnification

examinations, the product synthesized by high pressure and high temperature has some gray part, which is the synthesized  $MnB_2$  specimen, and some black part, which is the excess amorphous boron verified by EDS measurements. The corresponding chemical composition analyses of the gray parts yield  $Mn_{0.95}B_2$  as determined from the EDS measurements. The high-magnification SEM image, Figure 3b, show the

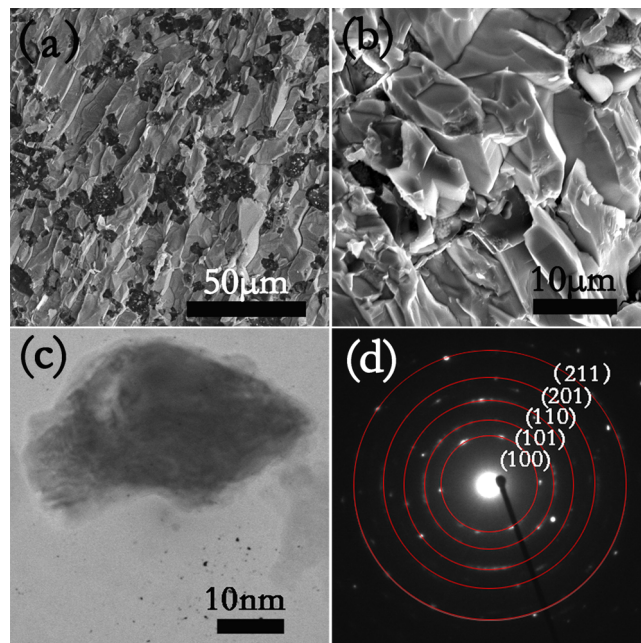


**Figure 3.** (a) Low- and (b) high-magnification SEM images of the as-obtained pure  $MnB_2$  bulk materials. (c) The bright-field TEM image of  $MnB_2$ . (d) SAED images of  $MnB_2$ .

gray parts microstructure of the synthesized polycrystalline hexagonal  $AlB_2$ -type  $MnB_2$ . The obtained specimen was nearly free of visible microcracks with an average grain size of  $\sim 10$ – $15$   $\mu m$ . Further characterization of the synthesized specimen was performed by the SAED, Figure 3d, and the HRTEM, Figure 2b. The obtained SAED circular pattern denotes its polycrystalline nature. The interplanar distance calculated from the crystal lattice fringes of HRTEM is 2.65 Å, shown in Figure 2b, which is corresponding to the distance between two (010) planes. Enlarged HRTEM shown in the inset exhibits hexagonal structure reflecting its honeycomb boron atomic configuration.

Electronic configuration is the key to exploring the origin of honeycomb boron layers, and it is vital to explain its physical properties. The XPS combined with first-principle calculation is one of the most promising methods to study electronic configuration.<sup>14</sup> Therefore, XPS and first-principle calculation were conducted. Figure 4a shows the B-1s spectrum with the binding energy from 181.0 to 201.0 eV, and Figure 4b shows the Mn-2p XPS spectrum with the binding energy from 635.0 to 655.0 eV. Two peaks emerged in the B-1s spectrum, and the unsymmetric spectrum was deconvoluted by software. There are two B-1s states with binding energy of 188.4 and 187.9 eV. The boron elementary substance usually has a binding energy ranging from 187.3 to 187.9 eV.<sup>14,33</sup> The relatively low binding energy, 187.9 eV, is assigned to the unreacted amorphous boron that remained in the specimen, while the higher binding energy, 188.4 eV, is belonging to the graphene-like honeycomb boron layers.<sup>34</sup> This binding energy is compatible with the

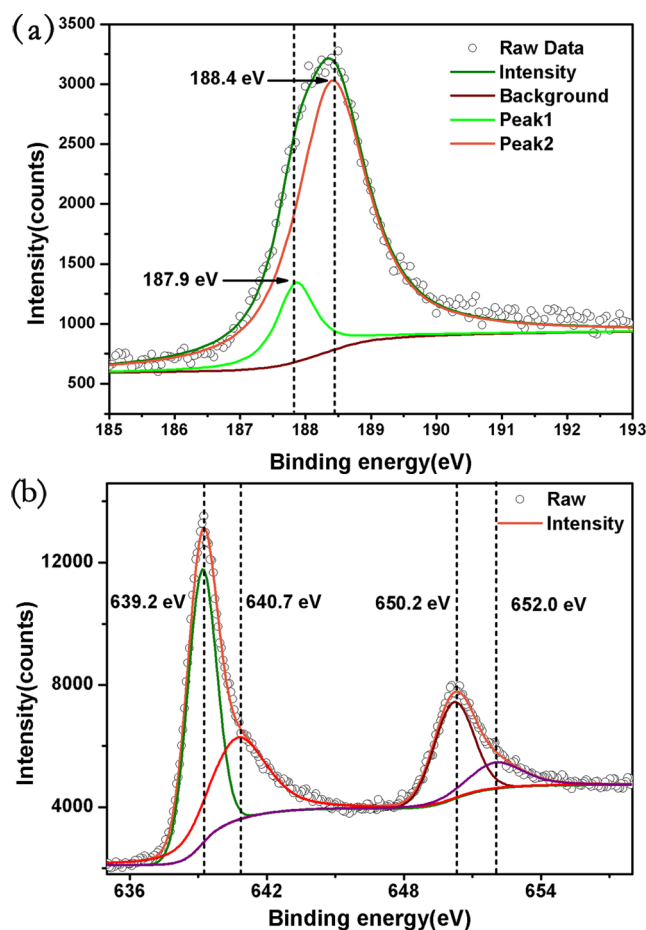


**Figure 4.** XPS spectra of  $\text{MnB}_2$  specimen synthesized by high pressure and high temperature, which was cleaned by the  $\text{Ar}^+$  sputtering with 180 s. (a) B-1s spectrum of  $\text{MnB}_2$  and (b) Mn  $2p^{3/2}$  and  $2p^{1/2}$  spectrum of  $\text{MnB}_2$ .

borophenes synthesized by Mannix et al.<sup>13</sup> As can be seen in the Mn-2p spectrum, the spectrum contains two major peaks at the binding energies of 639.2 and 650.2 eV, respectively. This binding energy is  $\sim 0.7$  eV higher than that of manganese metal.<sup>55</sup> Compared with elementary substance, higher binding energy signifies that there are some electrons transferred to boron atoms. The measured binding energy of Mn-2p is lower than other experimental results of 642.1 and 654.0 eV. The higher binding energy of V. V. Nemoshkalenko's result may stem from the oxidation states of manganese.<sup>33</sup>

However, there are two other peaks of Mn-2p with binding energy of 640.7 and 652.0 eV, respectively, which may be attributed to the defects of manganese that exist in the specimen. The boron atom has an electron configuration of  $[\text{He}]2s^2 2p^1$ . To form honeycomb graphene-like boron layers, one more electron is needed to fill the  $\pi$ -bands of honeycomb boron layer.<sup>18</sup> Transferring a certain amount of electrons from manganese atoms layers to boron atom 2p orbital is pivotal to form honeycomb boron layers. However, grabbing electron from manganese layers to boron will inevitably result in ionic bonds in Mn–B bonds, which are further investigated by first-principle calculations.

To assess the bonding nature between honeycomb boron layers and manganese layers, spin density of states (DOS) and electron location function (ELF) are calculated. From the DOS contour in Figure 5, there is an intriguing bonding situation

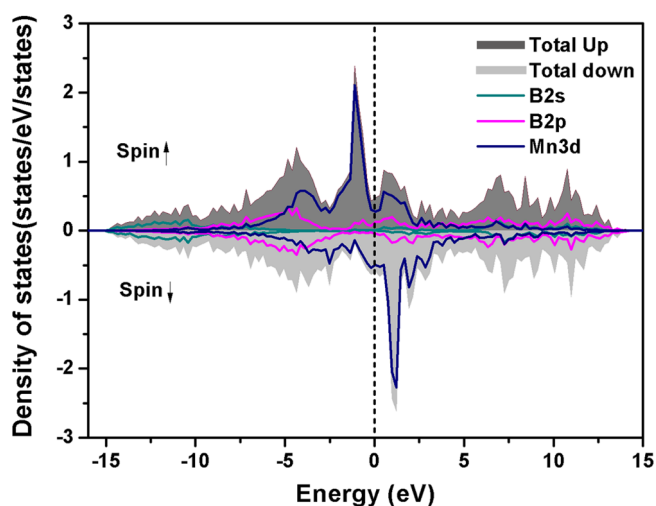


**Figure 5.** Spin-polarized DOS of  $\text{MnB}_2$ . The dark gray and light gray indicates spin-up and spin-down states, respectively.

that Mn and B forms only weak bonds as suggested by the mismatching of Mn-3d and B-2p curve shapes. This suggests the binding between two layers is loose, while other transition metal borides (TMBs) tend to be believed to possess strong hybridization between TMs d orbitals and boron 2p orbitals.<sup>56</sup> The typical feature of TM diborides DOS is the presence of pseudogap, which is generally considered as the result of hybridization between Mn 3d electrons and B 2p electrons. The presence of pseudogap in this ionic integrating layer structure reveals that pseudogap originates from B(2p)-B(2p) covalent interaction.<sup>27</sup> Furthermore, the finite electrons DOS at the Fermi energy level indicates a metallic feature of  $\text{MnB}_2$ . Integrating of the total spin up and spin down DOS to Fermi energy level gives magnetic moment of Mn atoms. The obtained magnetic moment is  $1.84 \mu_B/\text{Mn}$ . Assuming that the orbital moment is frozen, then, the effective  $\mu_{\text{eff}} = 2\mu_B \sqrt{S(S+1)}$  is  $\sim 2.66 \mu_B$ , which is comparable to the magnetic moment calculated from NMR experiment results.<sup>37</sup> Presence of electrical conductivity and magnetic property endow this sandwiching honeycomb structure to be potential multifunctional materials. Besides, more intriguing versatile properties, like spintronics, catalytic, and Dirac cone, are expected to be revealed in this bulk or 2D material.

Figure 6a–c highlights the sliced planes containing B–B bonds, Mn–Mn bonds, and Mn–B bonds, respectively. Figure 6d–f displays their corresponding ELF contours. In the honeycomb boron planes, high ELF distribution centers are on the middle of B–B atoms, indicating that there is a strong directional covalent  $\sigma$  bond similar to that of graphite.<sup>2</sup> In the manganese laminar layers, the electron distributes “jellium” like metallic electronic structure. However, in the planes containing Mn–B bonds, there is significant contrast of electron localization functions between B atoms and Mn atoms reflecting the ionic feature of Mn–B bonds. The electron transfer was verified by the Milliken atomic populations, and there are 1.19 electrons transferred from Mn to B, which implies every B obtains 0.59 electrons. Electron transferring from Mn to B fills the empty  $\pi$ -bands and stabilizes its honeycomb structure.<sup>38</sup> Milliken bond populations are 0.96 and 0 of B–B bonds in the honeycomb boron layers and Mn–B bonds between honeycomb boron and manganese layers, respectively. The high Milliken bond population between B–B

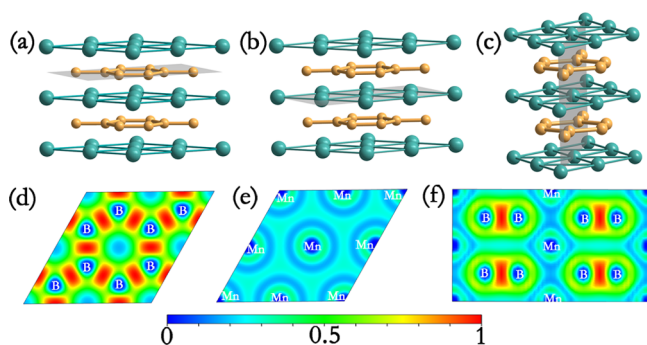


**Figure 6.** Bond mechanism of honeycomb boron sheets sandwiching manganese layers. (a–c) Cutting slabs along the B–B bonds, Mn–Mn bonds and Mn–B bonds plane, respectively. (d–f) Their corresponding ELF.

chemically reveals its strong directional covalent bond nature, while the Milliken bond population between Mn–B is zero signifying its soft ionic feature. This bonds strength configuration inevitably will result in strong anisotropy in the mechanical strength. Elastic constants  $C_{11}$  in the (001) plane is 602.5 GPa and  $C_{33}$  along the  $c$ -axis is only 387.6 GPa, which denotes the strong character of honeycomb boron layers. The obtained bulk modulus and shear modulus is 260.3 and 165.7 GPa, respectively. Owing to the high density of valence electrons, 0.55 electrons/Å<sup>3</sup>, MnB<sub>2</sub> possesses high bulk modulus. Compared with other TM B<sub>2</sub>, the relatively low shear modulus of MnB<sub>2</sub> implies its low ability to resist strain along  $c$  plane.

Neutron diffraction of MnB<sub>2</sub> with the temperature ranging from 5 to 298 K gives the equations of lattice parameters as a function of temperature,  $a = 3.004 + (4.9 \times 10^{-6})T$  and  $c = 3.0358 + (2 \times 10^{-6})T + (7 \times 10^{-8})T^2$ .<sup>39</sup> This result demonstrates that  $c$ -axis is more facile to change with temperature. Meng et al. report lattice parameters of MnB<sub>2</sub> as a function of pressure from experiment, and the result shows that there is larger changing of  $c$ -axis with the increasing pressure.<sup>40</sup> The observation of effortless change of  $c$ -axis with pressure is consistent with the conclusion arrived from the neutron diffraction measurements and first-principle calculations. The anisotropic thermal expansion of MnB<sub>2</sub> and lattice parameters with the increasing pressure indicate that Mn–B bonds in (001) directions, with respect to B–B bonds, is more facile to change with temperature and pressure. However, for most of the laminar TM light element compounds, the  $c$ -axis direction is more stable with the external factors, which may denote that the bonds in (001) direction are weaker than that in  $ab$  plane.<sup>41,42</sup> There are Mn–B bonds in the (001) directions and B–B covalent bonds combined with Mn–Mn metallic bonds in the  $c$ -planes. Those results demonstrate that Mn–B bond has relatively soft ionic character with respect to B–B covalent feature in  $c$ -planes, while other TM diborides have a relatively strong TM–B bond in the (001) directions. This bond peculiarity may originate from the high difference of electronegativity between manganese and boron.

Generally, bond strength anisotropy inevitably will generate hardness anisotropy between different crystal planes. The hardness of the synthesized polycrystalline specimen was measured by means of Vickers indentation method utilizing a pyramid-like diamond indenter to press an indentation on the gray parts. At each applied load of 0.245, 0.49, 0.98, 1.96, 2.94, and 4.9 N, at least five indentations were made to obtain an

average Vickers hardness value with dwell time of 15 s. However, the excess boron will give rise to an error in the Vicker's hardness measurement. Considering that measuring the hardness of specimens with excess amorphous boron usually leads to higher hardness value than the polycrystalline specimen's real hardness, it is necessary to eliminate the influence of excess boron on the hardness testing. To measure the hardness accurately, the diamond indenter only presses an indentation on the MnB<sub>2</sub> but not on the amorphous boron. After the hardness was measured, the polished specimen was observed by the SEM equipped with energy-dispersive spectrometer. The chemical composition EDS mapping of the polished surface around the indentation was done after an integrated indentation as shown in the Figure S2 was found under the SEM microscope. Chemical composition measurements indicate that the indentations are exactly on MnB<sub>2</sub> areas.

The obtained hardness with the relation of applied load is shown in Figure 7 indicating that hardness decreases with the

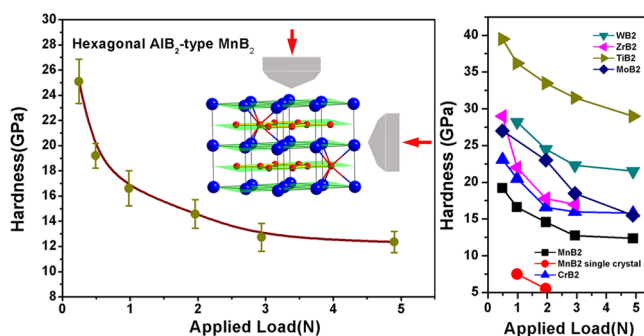


**Figure 7.** Vickers hardness of the as-synthesized MnB<sub>2</sub> sample as a function of applied load ranging from 0.245 N (low load) to 4.9 N (high load). The corresponding Vickers hardness ranging from 25.2 to 12.1 GPa at low load and high load, respectively. The experimental hardness of different TM diborides is shown at the right.<sup>44–48</sup>

increase of applied load. The maximum hardness at the applied load of 0.245 N is 25.1 GPa, and the asymptotic Vickers hardness is 12.3 GPa at the applied load of 4.9 N. Obviously, the hardness of polycrystalline MnB<sub>2</sub> specimen is 16.6 and 14.6 GPa at the applied loads of 0.98 and 1.96 N, respectively, which is harder than the corresponding value of 7.5 and 5.5 GPa of the single crystal at the same applied load. The higher hardness of polycrystalline specimen than that of single crystal is owing to the different crystal planes that the pyramid diamond indenter acts on. In general, there are different crystal planes under indenter in the polycrystalline specimen. Consequently, the hardness measurements on polycrystalline specimen are the average hardness of different crystal planes. Lower hardness of single-crystal hardness testing of Gou et al. is indented on the crystal planes perpendicular to the  $c$ -axis because of the slipping between honeycomb boron planes and manganese planes.<sup>43</sup> The strong hardness anisotropy of different crystal plane also demonstrates the strong anisotropy of bond strength in MnB<sub>2</sub>. Despite the anisotropy hardness, it is expected that there is high hardness value in  $c$ -direction. This remarkable hardness property in  $c$ -axis may be suitable for protective coatings, where direction-dependent hardness is favored. For most of AlB<sub>2</sub>-type TM diborides, the higher hardness is caused by the stronger TM–B bonds because of the strong hybridization of  $d$ -states and  $p$ -states. Different hybridization situation roots in the high electronegativity difference between Mn and B.

## CONCLUSIONS

Graphene-like honeycomb boron layers have been successfully stabilized by grabbing electrons from manganese layers.  $\text{MnB}_2$  is an extraordinary prototype of this type of sandwich structure exhibiting electronic conductivity and ferromagnetism. The high anisotropy of hardness, different axis compression ratios, and thermal expansion indicates that the mechanical strength of honeycomb boron sheets is rather high, which is useful in industrial application. The chemical bond Mn–B is a relatively soft ionic feature, which contradicts previous results that there is a strong hybridization between metal 3d electrons and B 2p electrons. This structure provides a platform to investigate the electronic quantum phenomenon, and it may have potential broad applications.

## ASSOCIATED CONTENT

### Supporting Information

The Supporting Information is available free of charge on the ACS Publications website at DOI: 10.1021/acs.inorgchem.6b01685.

Listings of X-ray diffraction data, scanning electron microscope EDS mapping data (PDF)

## AUTHOR INFORMATION

### Corresponding Author

\*E-mail: [cuitian@jlu.edu.cn](mailto:cuitian@jlu.edu.cn).

### Notes

The authors declare no competing financial interest.

## ACKNOWLEDGMENTS

This work was supported by the National Basic Research Program of China (No. 2011CB808200), National Natural Science Foundation of China (Nos. 51572108 and 51032001), Program for Changjiang Scholars and Innovative Research Team in Univ. (No. IRT1132), and National Found for Fostering Talents of Basic Science (No. J1103202).

## REFERENCES

- (1) Castro Neto, A. H.; Guinea, F.; Peres, N. M. R.; Novoselov, K. S.; Geim, A. K. The electronic properties of graphene. *Rev. Mod. Phys.* **2009**, *81*, 109–162.
- (2) Zhang, L. M.; Yu, J. W.; Yang, M. M.; Xie, Q.; Peng, H. L.; Liu, Z. F. Janus graphene from asymmetric two-dimensional chemistry. *Nat. Commun.* **2013**, *4*, 1443.
- (3) Jungthawan, S.; Reunchan, P.; Limpijumng, S. Theoretical study of strained porous graphene structures and their gas separation properties. *Carbon* **2013**, *54*, 359–364.
- (4) Vogt, P.; de Padova, P.; Quaresima, C.; Le Lay, G.; et al. Silicene: Compelling experimental evidence for graphenelike two-dimensional silicon. *Phys. Rev. Lett.* **2012**, *108*, 155501.
- (5) Zhu, Y.; Li, L.; Zhang, C. G.; Casillas, G.; Sun, Z. Z.; Yan, Z.; Ruan, G. D.; Peng, Z. W.; Raji, A. O.; Kittrell, C.; Hauge, R. H.; Tour, J. M. A seamless three-dimensional carbon nanotube graphene hybrid material. *Nat. Commun.* **2012**, *3*, 1225.
- (6) Huang, W.; Sergeeva, A. P.; Zhai, H. J.; Averkiev, B. B.; Wang, L. S.; Boldyrev, A. I. A concentric planar doubly  $\pi$ -aromatic  $\text{B}_{19}$ -cluster. *Nat. Chem.* **2010**, *2*, 202–206.
- (7) Chhowalla, M.; Shin, H. S.; Eda, G.; Li, L. J.; Loh, K. P.; Zhang, H. The chemistry of two-dimensional layered transition metal dichalcogenide nanosheets. *Nat. Chem.* **2013**, *5*, 263–275.
- (8) Ma, F. X.; Jiao, Y. L.; Gao, G. P.; Gu, Y. T.; Bilic, A.; Chen, Z. F.; Du, A. J. Graphene-like two-dimensional ionic boron with double dirac cones at ambient condition. *Nano Lett.* **2016**, *16*, 3022–3028.
- (9) Zhai, H. J.; Kiran, B.; Li, J.; Wang, L. S. Hydrocarbon analogues of boron clusters planarity, aromaticity and antiaromaticity. *Nat. Mater.* **2003**, *2*, 827–833.
- (10) Boustani, I.; Quandt, A.; Hernández, E.; Rubio, A. New boron based nanostructured materials. *J. Chem. Phys.* **1999**, *110*, 3176–3185.
- (11) Wu, X. J.; Dai, J.; Zhao, Y.; Zhuo, Z. W.; Yang, J. L.; Zeng, X. C. Two-dimensional boron monolayer sheets. *ACS Nano* **2012**, *6*, 7443–7453.
- (12) Evans, M. H.; Joannopoulos, J. D.; Pantelides, S. T. Electronic and mechanical properties of planar and tubular boron. *Phys. Rev. B: Condens. Matter Mater. Phys.* **2005**, *72*, 045434.
- (13) Mannix, A. J.; Zhou, X. F.; Kiraly, B.; Wood, J. D.; Alducin, D.; Guisinger, N. P.; et al. Synthesis of borophenes: Anisotropic two-dimensional boron polymorphs. *Science* **2015**, *350*, 1513–1516.
- (14) Ihara, H.; Hirabayashi, M.; Nakagawa, H. Band structure and x-ray photoelectron spectrum of  $\text{ZrB}_2$ . *Phys. Rev. B* **1977**, *16*, 726–730.
- (15) Zhang, L. Z.; Wang, Z. F.; Du, S. X.; Gao, H. J.; Liu, P. Prediction of a dirac state in monolayer  $\text{TiB}_2$ . *Phys. Rev. B: Condens. Matter Mater. Phys.* **2014**, *90*, 161402.
- (16) Li, Q.; Zhou, D.; Zheng, W. T.; Ma, Y. M.; Chen, C. F. Anomalous stress response of ultrahard  $\text{WB}_n$  compounds. *Phys. Rev. Lett.* **2015**, *115*, 185502.
- (17) Nagamatsu, J.; Nakagawa, N.; Muranaka, T.; Zenitani, Y.; Akimitsu, J. Superconductivity at 39 K in magnesium diboride. *Nature* **2001**, *410*, 63–64.
- (18) Xie, S. Y.; Li, X. B.; Tian, W. Q.; Chen, N. K.; Zhang, X. L.; Wang, Y. L.; Zhang, S. B.; Sun, H. B. First-principles calculations of a robust two-dimensional boron honeycomb sandwiching a triangular molybdenum layer. *Phys. Rev. B: Condens. Matter Mater. Phys.* **2014**, *90*, 035447.
- (19) Cadeville, M. C. Propriétés magnétiques des diborures de manganèse et de chrome  $\text{MnB}_2$  et  $\text{CrB}_2$ . *J. Phys. Chem. Solids* **1966**, *27*, 667–670.
- (20) Seo, W. S.; Jo, H. H.; Lee, K.; Kim, B.; Oh, S. J.; Park, J. T. Size-dependent magnetic properties of colloidal  $\text{Mn}_3\text{O}_4$  and  $\text{MnO}$  nanoparticles. *Angew. Chem., Int. Ed.* **2004**, *43*, 1115–1117.
- (21) Seiro, S.; Koller, E.; Fasano, Y.; Fischer, Ø. Homogeneous strain-relaxation effects in  $\text{La}_{0.67}\text{Ca}_{0.33}\text{MnO}_3$  films grown on  $\text{NdGaO}_3$ . *Appl. Phys. Lett.* **2007**, *91*, 091913.
- (22) Zhu, H.; Ni, C. Y.; Zhang, F. M.; Du, Y. W.; Xiao, J. Q. Fabrication and magnetic property of  $\text{MnB}$  alloy. *J. Appl. Phys.* **2005**, *97*, 10M512.
- (23) Salamon, M. B.; Herman, R. M. Critical dynamics and spin relaxation in a Cu–Mn Spin Glass. *Phys. Rev. Lett.* **1978**, *41*, 1506–1509.
- (24) Niu, H. Y.; Chen, X. Q.; Ren, W. J.; Zhu, Q.; Oganov, A. R.; Li, D. Z.; Li, Y. Y. Variable-composition structural optimization and experimental verification of  $\text{MnB}_3$  and  $\text{MnB}_4$ . *Phys. Chem. Chem. Phys.* **2014**, *16*, 15866–15873.
- (25) Wang, B.; Li, X.; Wang, Y. X.; Tu, Y. F. Phase stability and physical properties of manganese borides: A first-principle study. *J. Phys. Chem. C* **2011**, *115*, 21429–21435.
- (26) Aydin, S.; Simsek, M. First-principle calculations of  $\text{MnB}_2$ ,  $\text{TcB}_2$ , and  $\text{ReB}_2$  within the  $\text{ReB}_2$ -type structure. *Phys. Rev. B: Condens. Matter Mater. Phys.* **2009**, *80*, 134107.
- (27) Vajeeston, P.; Ravindran, P.; Ravi, C.; Asokamani, R. Electronic structure, bonding, and ground-state properties of  $\text{AlB}_2$ -type transition-metal diborides. *Phys. Rev. B: Condens. Matter Mater. Phys.* **2001**, *63*, 045115.
- (28) Kresse, G.; Furthmüller, J. Efficient iterative schemes for ab initio total-energy calculations using a plane-wave basis set. *Phys. Rev. B: Condens. Matter Mater. Phys.* **1996**, *54*, 11169–11186.
- (29) Perdew, J. P.; Burke, K.; Ernzerhof, M. Generalized gradient approximation made simple. *Phys. Rev. Lett.* **1996**, *77*, 3865–3868.
- (30) Segall, M. D.; Lindan, P. J. D.; Probert, M. J.; Pickard, C. J.; Hasnip, P. J.; Clark, S. J.; Payne, M. C. First-principles simulation: ideas, illustrations and the CASTEP code. *J. Phys.: Condens. Matter* **2002**, *14*, 2717–2744.

- (31) Segall, M. D.; Shah, R.; Pickard, C. J.; Payne, M. C. Population analysis of plane-wave electronic structure calculations of bulk materials. *Phys. Rev. B: Condens. Matter Mater. Phys.* **1996**, *54*, 16317–16320.
- (32) Shein, I. R.; Ivanovskii, A. L. Elastic properties of mono- and polycrystalline hexagonal  $AlB_2$ -like diborides of s, p and d metals from first-principles calculations. *J. Phys.: Condens. Matter* **2008**, *20*, 415218.
- (33) Nemoshkalenko, V. V.; Shashkina, T. B.; Aljeshin, V. G.; Senkevich, A. I. On the charge distribution in manganese borides studied by x-ray photoelectron and emission spectroscopy. *J. Phys. Chem. Solids* **1975**, *36*, 37–40.
- (34) Jiang, C. L.; Pei, Z. L.; Liu, Y. M.; Xiao, J. Q.; Gong, J.; Sun, C. Preparation and characterization of superhard  $AlB_2$ -type  $WB_2$  nanocomposite coatings. *Phys. Status Solidi A* **2013**, *210*, 1221–1227.
- (35) Jenks, C. J.; Chang, S. L.; Anderegg, J. W.; Thiel, P. A.; Lynch, D. W. Photoelectron spectra of an  $Al_{70}Pd_{21}Mn_9$  quasicrystal and the cubic alloy  $Al_{60}Pd_{25}Mn_{15}$ . *Phys. Rev. B: Condens. Matter Mater. Phys.* **1996**, *54*, 6301–6306.
- (36) Levine, J. B.; Tolbert, S. H.; Kaner, R. B. Advancements in the search for superhard ultra-incompressible metal borides. *Adv. Funct. Mater.* **2009**, *19*, 3519–3533.
- (37) Kasaya, M.; Hihara, T.; Kōi, Y. NMR study in  $MnB_2$ . *J. Phys. Soc. Jpn.* **1969**, *26*, 1549.
- (38) Peng, F.; Miao, M. S.; Wang, H.; Li, Q.; Ma, Y. M. Predicted Lithium-boron compounds under high pressure. *J. Am. Chem. Soc.* **2012**, *134*, 18599–18605.
- (39) Bowman, A. L.; Nereson, N. G. Low-temperature thermal expansion of  $MnB_2$ . *AIP Conf. Proc.* **1973**, *17*, 34.
- (40) Meng, X. X.; Fan, J.; Bao, Z.; Zhu, P. W.; Cui, T.; et al. Structural stability and electrical properties of  $AlB_2$ -type  $MnB_2$  under high pressure. *Chin. Phys. B* **2014**, *23*, 016102.
- (41) Cumberland, R. W.; Weinberger, M. B.; Gilman, J. J.; Clark, S. M.; Tolbert, S. H.; Kaner, R. B. Osmium diboride, an ultra-incompressible, hard material. *J. Am. Chem. Soc.* **2005**, *127*, 7264–7265.
- (42) Chung, H. Y.; Weinberger, M. B.; Levine, J. B.; Kavner, A.; Yang, J. M.; Tolbert, S. H.; Kaner, R. B. Synthesis of ultra-incompressible superhard rhenium diboride at ambient pressure. *Science* **2007**, *316*, 436–439.
- (43) Gou, H. Y.; Steinle-Neumann, G.; Bykova, E.; Nakajima, Y.; Miyajima, N.; Li, Y.; Ovsyannikov, S. V.; Dubrovinsky, L. S.; Dubrovinskaya, N. Stability of  $MnB_2$  with  $AlB_2$ -type structure revealed by first-principles calculations and experiments. *Appl. Phys. Lett.* **2013**, *102*, 061906.
- (44) Li, J. J.; Zhao, X. P.; Tao, Q.; Huang, X. Q.; Zhu, P. W.; Cui, T.; Wang, X. Characterization of  $TiB_2$  synthesized at high pressure and high temperature. *Acta Phys. Sin.* **2013**, *62*, 026202.
- (45) Wang, S.; Yu, X.; Zhang, J.; Zhang, Y.; Wang, L.; Leinenweber, K.; Xu, H.; Popov, D.; Park, C.; Yang, W.; He, D.; Zhao, Y. Crystal structures, elastic properties, and hardness of high-pressure synthesized  $CrB_2$  and  $CrB_4$ . *J. Superhard Mater.* **2014**, *36*, 279–287.
- (46) Tao, Q.; Zhao, X. P.; Chen, Y. L.; Li, J.; Li, Q.; Ma, Y. M.; Li, J. J.; Cui, T.; Zhu, P. W.; Wang, X. Enhanced vickers hardness by quasi-3D boron network in  $MoB_2$ . *RSC Adv.* **2013**, *3*, 18317–18322.
- (47) Yin, S.; He, D. W.; Xu, C.; Wang, W. D.; Zhu, W. J.; et al. Hardness and elastic moduli of high pressure synthesized  $MoB_2$  and  $WB_2$  compacts. *High Pressure Res.* **2013**, *33*, 409–417.
- (48) Nakamori, F.; Ohishi, Y.; Muta, H.; Kurosaki, K.; Fukumoto, K.; Yamanaka, S. Mechanical and thermal properties of bulk  $ZrB_2$ . *J. Nucl. Mater.* **2015**, *467* (612), 617.